Theoretical Modeling of Hydroxyl−Radical-Induced Lipid Peroxidation Reactions

ARTICLE *in* THE JOURNAL OF PHYSICAL CHEMISTRY B · JUNE 2007

Impact Factor: 3.3 · DOI: 10.1021/jp0650782 · Source: PubMed

Theoretical Modeling of Hydroxyl-Radical-Induced Lipid Peroxidation Reactions

Ismael Tejero,[†,‡] Àngels González-Lafont,[†] José M. Lluch,[†] and Leif A. Eriksson*[,‡]

Departament de Química, Universitat Autònoma de Barcelona, 08193 Bellaterra, Barcelona, Spain, and Department of Natural Sciences and Örebro Life Science Center, Örebro University, 701 82 Örebro, Sweden

Received: August 7, 2006; In Final Form: March 12, 2007

The OH-radical-induced mechanism of lipid peroxidation, involving hydrogen abstraction followed by O_2 addition, is explored using the kinetically corrected hybrid density functional MPWB1K in conjunction with the MG3S basis set and a polarized continuum model to mimic the membrane interior. Using a small nonadiene model of linoleic acid, it is found that hydrogen abstraction preferentially occurs at the mono-allylic methylene groups at the ends of the conjugated segment rather than at the central bis-allylic carbon, in disagreement with experimental data. Using a full linoleic acid, however, abstraction is correctly predicted to occur at the central carbon, giving a pentadienyl radical. The Gibbs free energy for abstraction at the central C_{11} is ∼8 kcal/mol, compared to 9 kcal/mol at the end points (giving an allyl radical). Subsequent oxygen addition will occur at one of the terminal atoms of the pentadienyl radical fragment, giving a localized peroxy radical and a conjugated butadiene fragment, but is associated with rather high free energy barriers and low exergonicity at the CPCM-MPWB1K/MG3S level. The ZPE-corrected potential energy surfaces obtained without solvent effects, on the other hand, display considerably lower barriers and more exergonic reactions.

1. Introduction

Lipid peroxidation is one of the main deleterious effects resulting from the exposure of living organisms to high energy radiation and reactive oxygen species (ROS). It is the essential cause of many pathobiological processes such as atherosclerosis, carcinogenesis, and cell death.[1,2] Oxidative stress induces damage to many biological molecules, including membrane lipids, proteins, and DNA, the latter being the most significant targets of injury.[3,4]

For the last two decades, the hypothesis of oxidation leading to atherosclerosis has stimulated extensive studies on the oxidative modification of the low density lipoprotein (LDL), the main source of cholesterol.[5] Oxidative stress in vivo has also received a great deal of attention in connection with the oxidation of polyunsaturated fatty acids (PUFA). In addition, both PUFA and cholesterol can be oxidized by enzymatic as well as nonenzymatic pathways.

Free radicals attack any PUFA with essentially equal probability, and do not discriminate between esterified or free acids. Since the amount of linoleic acid (LA) exceeds that of arachidonic acid (AA) by more than 1 order of magnitude in biological samples,[6] it is commonly accepted to consider lipid peroxidation in vivo to mainly involve LA.[7]

In lipoxygenase enzymes, the oxidation of linoleic acid proceeds catalytically via a hydrogen abstraction from the activated bis-allylic CH_2 group in a highly regiospecific and stereospecific reaction.[8−10] The lipid radical formed adds oxygen at the end of the delocalized system, producing exclusively one chiral hydroperoxy octadecadienoic acid (HPODE). The current study, however, focuses on the nonenzymatic pathway, in which the stereochemistry and mode of action is much less controlled.

Nonradical and nonenzymatic lipid peroxidation mechanisms involving, for example, singlet oxygen are also well established, and have been the subject of detailed experimental and theoretical studies.[11−13] In the late 1980s, Cosgrove et al.[14] found that the oxidizability of PUFA is linearly dependent on the number of bis-allylic methylenes present in the fatty acid. As can be observed in Scheme 1, it seems reasonable that oxidizability is controlled by the initial event of hydrogen abstraction by radicals from the relatively weak C−H bond of the bis-allylic methylene (bond dissociation energy, BDE, ∼75 kcal/mol). For mono-unsaturated lipids, like oleic acid, the oxidizability is much reduced, since the mono-allylic methylene hydrogens (C−H BDE ∼88 kcal/mol) are more resistant to abstraction.[15]

Once the PUFA radical is formed, the unpaired spin density will be delocalized over the conjugated region, in an odd-alternant fashion. The major components of unpaired spin in the C_{11}-dehydrogenated dienyl radical will thus be found on carbons C_9, C_{11}, and C_{13} (cf. Scheme 1). Molecular oxygen will primarily attack these sites, and in particular those at the end points (C_9 and C_{13}) of the delocalized system, to form a peroxyl radical. The lipid peroxyl radical (LOO•) may then abstract a hydrogen atom from an adjacent lipid molecule, leading to a propagation of the peroxidation sequence. The propagating lipid peroxidation may terminate by cross-link formation between lipid side chains, or via lipid−protein cross-links, which hence reduce the fluidity and transport properties of the membrane, or the mobility and action of membrane bound proteins. Another fate of the lipid peroxyl radicals is the formation of cyclic peroxides that in turn can degrade via hydrolysis or heat to give strongly mutagenic malondialdehyde (MDA) or 4-hydroxy-2-nonenal, and/or other more or less toxic products.[16,17] The cyclic endoperoxides can also lead to isoprostane formation, which are often associated with reduced kidney blood flow and development of kidney failure.[18,19] Increased understanding of the underlying mechanistic aspects of lipid peroxidation may assist in our understanding of the prevention of its toxic side effects.

* Corresponding author. E-mail: leif.eriksson@nat.oru.se.
† Universitat Autònoma de Barcelona.
‡ Örebro University.

10.1021/jp0650782 CCC: $37.00
Published on Web 05/02/2007

SCHEME 1: General Mechanism of Initiation and Propagation of Lipid Peroxidation

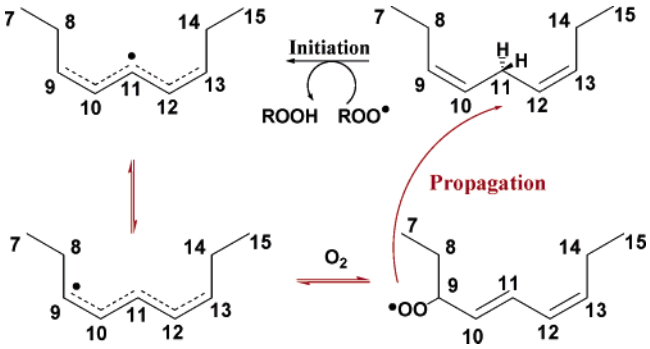

In the current study, we focus on the first two steps of lipid peroxidation induced by a free radical nonenzymatic pathway. Just as for lipoxygenase enzymes, ROS, and in particular hydroxyl radical, are capable of abstracting hydrogens from LA; however, as opposed to the enzymatic reactions, these radicals could remove hydrogens not only from bis-allylic CH_2 groups (position C_{11}) but also from methylene groups with only one adjacent double bond (positions C_8/C_{14}).[20] The aim of the study is to provide the first theoretical insight into the explicit mechanisms of the OH-radical-initiated lipid peroxidation processes, whether these are governed by thermodynamics or kinetics, and if the local surrounding is capable of directing the reactions toward a certain pathway.

There are several sources of OH radicals within lipid membranes, such as radiolytic degradation of water molecules traversing the bilayer, photodynamic generation mediated by membrane dissolved senstitizers, or via Fenton chemistry of iron- or copper-containing membrane-bound enzymes.[21−23] As shown by Hideg and Vass in 1996, hydroxyl radicals are the first ROS generated in UV-B exposed isolated thylakoid membranes from spinach, and are independent of the presence of molecular oxygen (i.e., the observed hydroxyl radicals are not derived from serial conversion of superoxide via hydrogen peroxide into hydroxyl radicals).[24] OH radicals are among the strongest oxidizing agents, in part due to the high bond strength of the formed O−H bond in the resulting water molecule (∼120 kcal/mol). They are known to react indiscriminately with any substance in the close vicinity of their generation, and thus have very short lifetimes (in the order of nanoseconds).[1] Due to their high reactivity, the possibility to remove also the mono-allylic hydrogens (from C_8/C_{14} in LA) has been previously proposed.[1,14]

The competing reactions of, on the one hand, hydrogen abstraction by hydroxyl radicals and, on the other hand, direct OH addition to double bonds have been investigated in several model systems. In, for example, thymine, OH radicals can add to either carbon of the $C_5{=}C_6$ double bond or abstract a hydrogen from the C_5 methyl group (producing an allylic radical).[25] Addition to C_5 is the main pathway, but all three are energetically highly similar and all three products are observed. For pyridoxine (vitamin B_6), we have recently performed a very detailed study of all possible reactions leading to OH adducts or hydrogen abstraction by OH radicals.[26] It was there shown that H abstraction was favored, both kinetically and thermodynamically, over direct OH addition.

Very few theoretical studies can be found concerning the mechanistic aspects of lipid peroxidation. Rauk and co-workers have, in their computational study of the possible mechanism of peroxynitrite oxidation of aliphatic CH bonds, shown that the principal pathway for the oxidation of 1,4-pentadiene

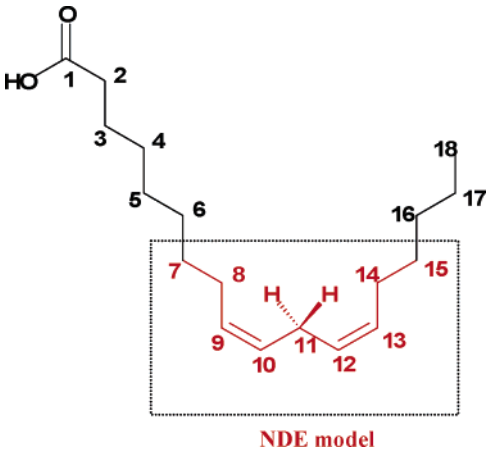

Figure 1. Linoleic acid and the nonadiene fragment thereof.

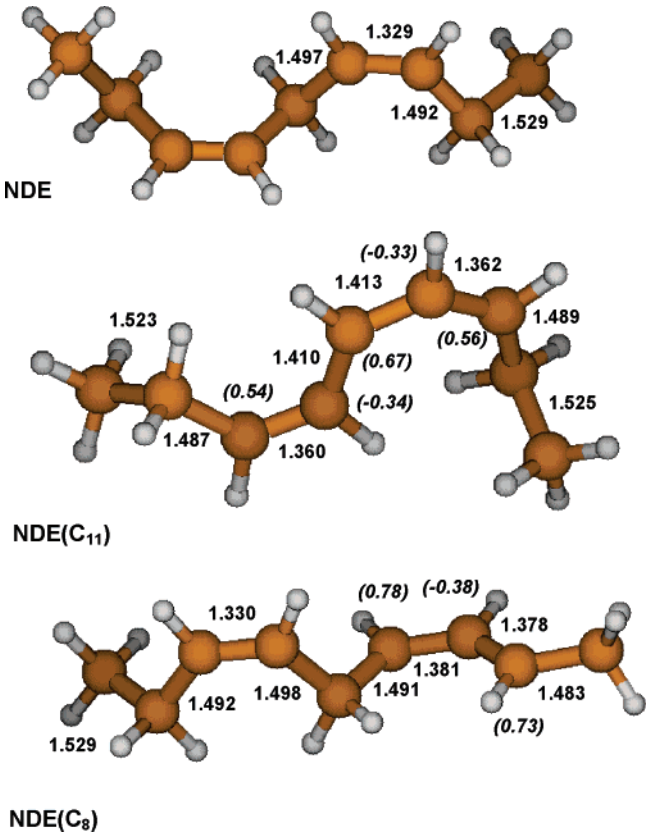

Figure 2. Optimized structures of lipid model NDE and pentadienylic NDE(C_{11}) and allylic NDE(C_8) H abstraction radicals. Distances in Å. Spin distributions (au) on the carbon atoms given in parentheses.

(a smaller model system for LA) by peroxynitrous acid (HNO_3) in the presence of air is via OH radicals produced upon homolysis of the O−O bond.[27] This fact emphasizes again the importance of OH radicals as the most susceptible and general ROS able to initiate a lipid peroxidation process.

2. Methodology

The initial lipid model employed in the current study is nona-3,6-diene (NDE), which represents the unsaturated fragment of linoleic acid with double bonds between carbon $C_9{=}C_{10}$ and $C_{12}{=}C_{13}$; see Figure 1. Geometry optimizations of all stationary points were performed within the hybrid density functional theory (DFT) framework.[28,29] The MPWB1K hybrid functional was used, which is a modified Perdew and Wang 1991 exchange

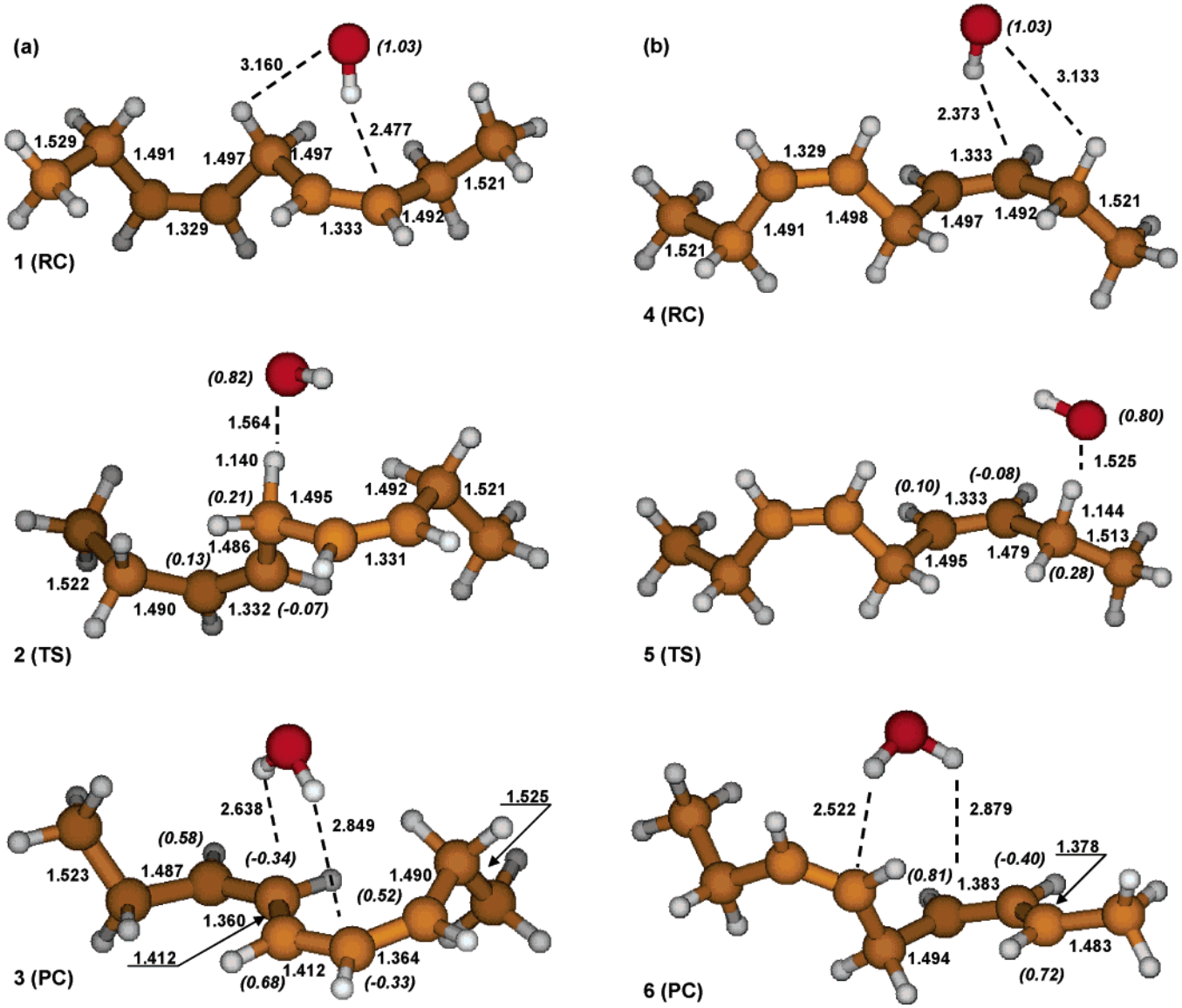

Figure 3. Optimized structures of reactant complexes, transition states, and product complexes for OH-induced H abstraction from the methylene group in NDE: (a) abstraction from bis-allylic C_{11}; (b) abstraction from mono-allylic C_8/C_{14}. Distances in Å. Spin distributions (au) given in parentheses.

TABLE 1: Energetics (in kcal/mol) Using High Level DFT/MG3S Calculations on the MPWB1K/6-31+G(d,p) Optimized Geometries for the Different H Abstractions Studied

reaction	compound	ΔE_{ZPE}[a] MPWB1K	$\Delta G^{298}_{vac.}$[a] MPWB1K	$\Delta G^{298}_{lip.}$[b] MPWB1K	$\Delta G^{298}_{lip.}$[b] B3LYP	$\Delta G^{298}_{lip.}$[b] BH&HLYP
H abstraction on C_{11}	NDE(C_{11}H) + OH•	0.0	0.0	0.0	0.0	0.0
	RC **1**	−2.2	5.1	8.4	9.0	8.8
	TS **2**	0.3	9.3	11.2	7.7	15.0
	PC **3**	−43.5	−34.2	−31.4	−32.0	−27.4
	NDE(C_{11}) + H_2O	−40.1	−40.4	−40.6	−42.9	−37.8
H abstraction on C_8/C_{14}	NDE(C_8H) + OH•	0.0	0.0	0.0	0.0	0.0
	RC **4**	−2.0	5.8	9.0	9.6	9.4
	TS **5**	−0.3	7.3	8.0	3.2	10.7
	PC **6**	−36.6	−29.3	−27.5	−28.0	−23.9
	NDE(C_8) + H_2O	−34.7	−36.5	−37.3	−39.5	−34.8

[a] Gas-phase calculations. [b] CPCM ($\epsilon = 4$) calculations.

functional[30] and Becke's 1995 meta correlation functional,[31] as developed by Truhlar et al.[32] Through the meta correlation functional, a dependence on the kinetic energy density is introduced, besides the "conventional" electron density and its gradient. The functional has recently been tested against kinetic databases and is shown to provide very accurate results for a combination of thermochemistry, kinetics, hydrogen bonding, and weak interactions.[33] It is particularly suitable for studies involving kinetics and noncovalent interactions, and has been shown to be very accurate in reproducing OH-induced hydrogen abstraction reactions in substituted alkanes and alkenes.[34]

The 6-31+G(d,p) basis set was used for the optimization calculations, and frequency calculations were performed at the same level of theory on the optimized stationary points in order

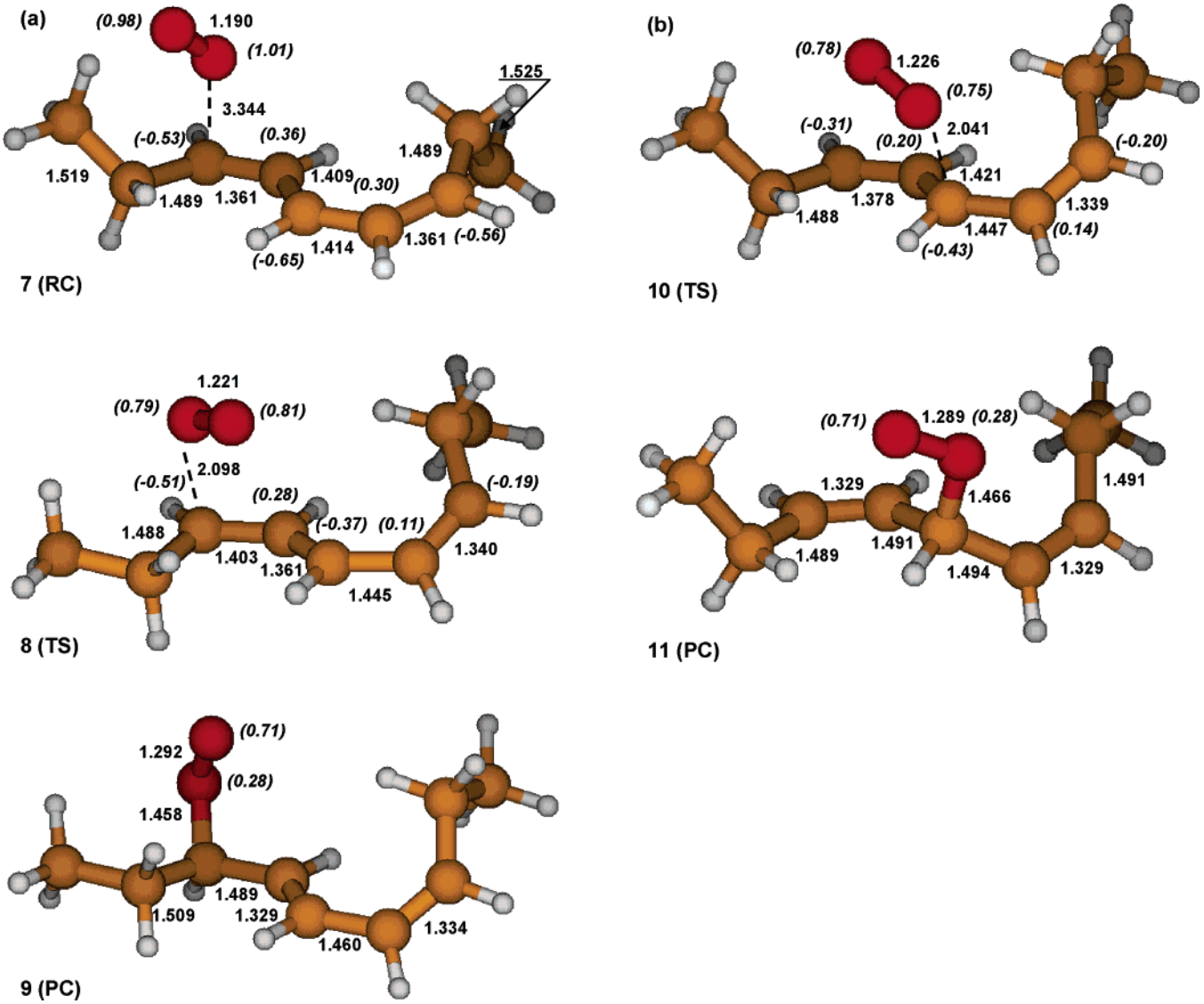

Figure 4. Optimized structures of reactant complexes, transition states, and product complexes for O_2 addition to the pentadienylic NDE(C_{11}) radical: (a) addition to C_9/C_{13}; (b) addition to "bis-allylic" C_{11}. Distances in Å. Spin distributions (au) given in parentheses.

to extract zero-point vibrational energy (ZPE) corrections and Gibbs free energies at 298 K and 1 atm of pressure, and to ensure that the located structures were either local minima or transition state structures on the potential energy surfaces.

Single-point energy calculations were subsequently performed at the MPWB1K/MG3S[35] level of theory, using the MPWB1K/6-31+G(d,p) optimized geometries, for additional estimations of Gibbs free energies of reaction. The MPWB1K/6-31+G(d,p) level of theory has been shown to give very good agreement with CCSD(T)/aug-cc-pVTZ calculations for OH-induced H abstraction reactions,[34] and the use of single-point calculations with the MG3S basis set was recommended as providing very good refinement of barrier heights.

The effects of bulk solvation were estimated through single-point energy calculations using the conductor-like formalism of Barone et al.,[36] at the MPWB1K/MG3S level. For the CPCM calculations, a value of 4 was employed for the dielectric constant, to simulate the hydrophobic interior of a lipid membrane. At all levels of theory employed, we find endergonic reaction complex (RC) formation (i.e., that the Gibbs free energies of the RCs lie higher in energy than the isolated reactants). Thus, we herein chose to primarily focus on free energies relative to the free reactants, rather than the optimized RCs, although the latter are important in order to locate the transition state structures of the various reactions.

Finally, since the MPWB1K level of theory is very recent, we also include results from single-point calculations with the MG3S basis set, using the conventional B3LYP and BH&HLYP functionals. The former is known to underestimate barriers, and the latter, due to the larger component of pure ("Hartree−Fock") exchange, notoriously overestimates these. All calculations are performed using the Gaussian 03 program package.[37]

3. Results and Discussion

3.1. OH-Radical-Induced H Abstraction. In the NDE system, we considered the two reactions in which the OH radical abstracts a lipid hydrogen from either a mono-allylic or a bis-allylic methylene group (C_8 or C_{11} of Figure 1, respectively). The optimized structures, key geometric parameters and spin distributions of the reactant complexes, transition state structures, and product complexes of the two reactions are displayed in Figures 2 and 3. In Table 1, we list the energetics of the different systems (ZPE-corrected energetics and Gibbs free energies in the gas phase, obtained at the MPWB1K/MG3S level; Gibbs free energies in solution at the MPWB1K, B3LYP, and

TABLE 2: Energetics (in kcal/mol) Using High Level DFT/MG3S Calculations on the MPWB1K/6-31+G(d,p) Optimized Geometries for the Different O_2 Additions Studied

reaction	compound	ΔE_{ZPE}[a] MPWB1K	$\Delta G^{298}_{vac.}$[a] MPWB1K	$\Delta G^{298}_{lip.}$[b] MPWB1K	$\Delta G^{298}_{lip.}$[b] B3LYP	$\Delta G^{298}_{lip.}$[b] BH&HLYP
O_2 addition to NDE(C_{11}) radical on C_9/C_{13}	NDE(C_{11}) + O_2	0.0	0.0	0.0	0.0	0.0
	RC **7**	−0.2	9.1	9.2	10.5	10.2
	TS **8**	6.4	17.3	14.7	12.9	19.8
	PC **9**	−11.2	−0.22	−2.6	2.6	2.3
O_2 addition to NDE(C_{11}) radical on C_{11}	NDE(C_{11}) + O_2	0.0	0.0	0.0	0.0	0.0
	RC **7**	−0.2	9.1	9.2	10.5	10.2
	TS **10**	7.2	18.9	17.7	15.1	24.4
	PC **11**	−6.7	5.3	2.6	7.6	7.5
O_2 addition to NDE(C_8) radical on C_8	NDE(C_8) + O_2	0.0	0.0	0.0	0.0	0.0
	RC **12**	0.0	7.4	7.6	7.8	7.8
	TS **13**	1.7	13.4	9.9	5.4	14.0
	PC **14**	−15.0	−4.4	−7.2	−3.8	−3.5
O_2 addition to NDE(C_8) radical on C_{10}	NDE(C_8) + O_2	0.0	0.0	0.0	0.0	0.0
	RC **15**	0.2	9.9	10.2	11.4	11.0
	TS **16**	13.8	24.1	14.5	10.0	23.9
	PC **17**	−16.1	−4.7	−8.0	−3.8	−3.7

[a] Gas-phase calculations. [b] CPCM ($\epsilon = 4$) calculations.

BH&HLYP levels with the MG3S basis set). All energies are given relative to the isolated reactants.

3.1.1. H Abstraction from the bis-Allylic Methylene NDE-($C_{11}H$). In the pathway NDE(C_{11}H) + OH → **1** → **2** → **3** → NDE(C_{11}) + H_2O (Figure 3a), the initial reactant complex **1** is formed through interaction between the hydroxylic hydrogen and the C_9-C_{10} π-cloud with distances around 2.5 Å, and with the O···H(C_{11}) distance being 3.16 Å. The unpaired electron is entirely localized to the hydroxylic oxygen. The TS **2** is an early transition state structure, as seen by the large difference in C−H (1.140 Å) and O···H bond distance (1.564 Å) and by the fact that the C−C bonds in the lipid are essentially unaltered. The unpaired spin is shared primarily between the oxygen (0.82 au) and C_{11} (0.21 au). In the resulting product complex **3**, the formed water molecule interacts through its hydrogen atoms with the radical π-cloud. The radical displays an odd-alternant spin distribution, with 0.5−0.7 unpaired electrons on carbons C_9, C_{11}, and C_{13} and −0.3 au each on C_{10} and C_{12}. Radical carbons C_9 and C_{13} bridge to the saturated fragments with bond lengths of 1.49 Å (same as in the unreacted lipid), the former π-bonds C_9-C_{10} and $C_{12}-C_{13}$ are slightly longer than in the initial lipid (1.36 vs 1.33 Å), and the new conjugated bonds of the pentadienyl radical fragment, $C_{10}-C_{11}$ and $C_{11}-C_{12}$, have bond lengths halfway between these at 1.41 Å.

3.1.2. H Abstraction from the mono-Allylic Methylene NDE-(C_8H). The pathway NDE(C_8H) + OH → **4** → **5** → **6** → NDE-(C_8) + H_2O (Figure 3b) displays very similar features as those outlined above. The hydroxyl radical initially interacts with its oxygen to a hydrogen atom on C_8 (3.13 Å) and with its hydrogen to the C_9-C_{10} π-cloud ((O)H···C distances ca. 2.4 Å) in the reactant complex **4**. The TS **5** is again very early, with R_{C-H} = 1.144 Å and R_{H-O} = 1.525 Å, and with the unpaired spin shared between O (0.80 au) and C_8 (0.28 au). The radical in the product complex **6** is now centered on three carbons ($C_8-C_9-C_{10}$), which hence each display a larger spin population than that for the product **3** (0.72, −0.40, and 0.81 au, respectively).

The computed MPWB1K/MG3S + ZPE energies for the two reactions are given in Table 1. The two surfaces differ slightly in that abstraction at the allylic C_8 is associated with a small negative potential energy barrier (−0.3 kcal/mol) compared with the low positive value of 0.3 kcal/mol for abstraction at the bis-allylic C_{11}, but is less thermodynamically favored (ΔE_{ZPE} of the products is −40.1 kcal/mol for **3** but −34.7 kcal/mol for **6**). The inclusion of entropy and enthalpy raises the barriers, as well as various complex energies, by 7−9 kcal/mol, whereas the further addition of solvent effects destabilizes the system by approximately 1−3 kcal/mol. The CPCM-MPWB1K/MG3S level gives a Gibbs free energy barrier for H abstraction at C_{11} of 11.2 kcal/mol, whereas the barrier at C_8 remains lower (8.0 kcal/mol).

The same trends are seen when using the B3LYP or BH&HLYP functionals instead of MPWB1K, albeit the former of these gives much reduced barrier heights and the latter of the two gives barriers that are ∼3 kcal/mol higher than the MPWB1K data. This is also seen for the product complexes, where B3LYP gives more stable products and BH&HLYP gives less stable ones, whereas only small differences are observed for the reactant complexes. All calculations using NDE as the LA model hence point to the interesting fact that abstraction at a mono-allylic methylene group (C_8/C_{14}) is in fact associated with a lower barrier than abstraction at a bis-allylic site (C_{11}). This could have implications to the suggested feasibility of these reactions and is an important feature that will be addressed in more detail below.

3.2. O_2 Addition to the Lipid Radical Site. As shown in Scheme 1, once the radical site is generated on the lipid moiety, triplet molecular oxygen ($^3\Sigma_g$) can readily add, thereby generating a lipid peroxyl radical (LOO•). The peroxyl radical can, in turn, abstract a hydrogen from a neighboring lipid (giving the hydroperoxide form (LOOH) and a new carbon-centered lipid radical) which leads to a propagating peroxidation reaction, or it may ring-close into a cyclic endoperoxide which in turn can rearrange into isoprostanes or degrade into mutagenic malondialdehyde or other products. Following the general hypothesis about lipid peroxidation mechanisms, the addition of molecular oxygen to the carbon-centered lipid radical is generally depicted as occurring in the terminal carbons C_9 and C_{13}; cf. Scheme 1.

Previous theoretical studies of oxygen addition to the propargyl radical (C_3H_3) showed gas-phase adiabatic potential energy barriers in the range 2.5−8.2 kcal/mol depending on computational level (B3LYP/6-311+G(d,p), MCG3, and QCISD(T)/6-311++G(3df,2pd)), through two different reaction channels.[38] Addition to the allyl radical has also been investigated, and was assumed to proceed through a barrierless reaction on the basis of CBS-QB3 calculations in the gas phase (adiabatic barrier).[39]

3.2.1. Addition to the bis-Allylic Methylene NDE(C_{11}). The main spin populations in the NDE(C_{11}) lipid radical are found on C_9, C_{11}, and C_{13}. Hence, two different oxygen additions are possible, either to C_9/C_{13} (pathway NDE(C_{11}) + O_2 → **7** → **8** → **9**) or to the central C_{11} carbon (pathway NDE(C_{11}) + O_2 →

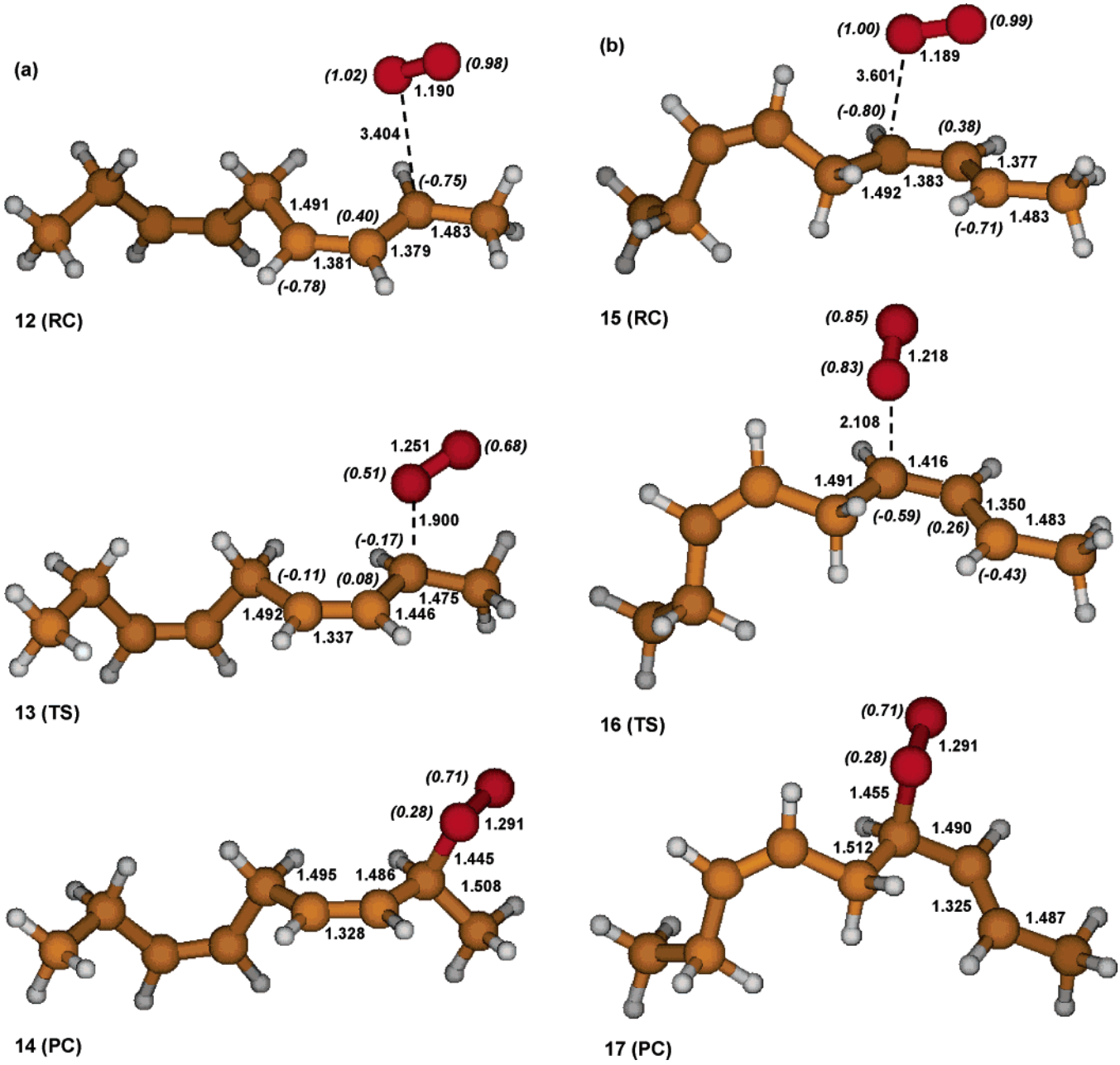

Figure 5. Optimized structures of reactant complexes, transition states, and product complexes for O_2 addition to the allylic NDE(C_8) radical: (a) addition to C_8; (b) addition to C_{10}. Distances are Å. Spin distributions (au) given in parentheses.

7 → **10** → **11**). Both of these reactions were found to have the same initial RC **7** (Figure 4a). In **7**, the unpaired spin of the lipid radical NDE(C_{11}) is essentially unaltered and the two oxygen atoms have one unpaired electron each. In TS **8** leading to addition to C_9, the interaction between one of the oxygen atoms and C_9 leads to a reduced spin population, ca. 1.6 unpaired electrons on the O_2 moiety and −0.68 au on the lipid radical fragment. The change in electronic structure is also manifested in the bond distances, mainly between the carbons in the C_9−C_{12} fragment (Figure 4a). In the product **9**, finally, the unpaired electron is found mainly on the oxygen atoms (0.71 and 0.28 electrons on the terminal and bridging oxygen, respectively), whereas the conjugated carbon fragment has attained a structure of a closed-shell butadiene.

TS **10**, for O_2 addition to the central carbon of the conjugated radical fragment C_{11}, is similar to **8** in that there is approximately 1.5 unpaired electrons on the oxygens and −0.6 au on the carbon fragment (Figure 4b). The C···O distance is just over 2 Å, as also seen in TS **8**. In this case, the changes in geometric features of the conjugated part are less dramatic, as the resulting species **11** contains two isolated π-bonds (between C_9−C_{10} and C_{12}−C_{13}), with the saturated C_{11} bridging these. The local spin distribution in the resulting LOO• radical **11** is identical to that in **9**.

In Table 2, we display the energetics of the two reaction paths for oxygen addition to NDE(C_{11}). The MPWB1K/MG3S + ZPE potential energy barrier height for addition to C_9/C_{13} (the hypothesized main site) is 6.4 kcal/mol, 0.8 kcal/mol lower than that for addition to C_{11}. The greater product stability, $\Delta\Delta E$ ∼4.5 kcal/mol, also speaks in favor of the formation of species **9** over **11**, and can be attributed to the resonance stabilization of butadiene compared to two isolated ethene fragments. As noted in the case of H abstraction, the inclusion of entropy and enthalpy has a dramatic effect on the energetics, raising the barriers by ∼11 kcal/mol. Adding solvent effects, finally, gives barriers of 15 kcal/mol for addition to C_9/C_{13} and 17.7 kcal/

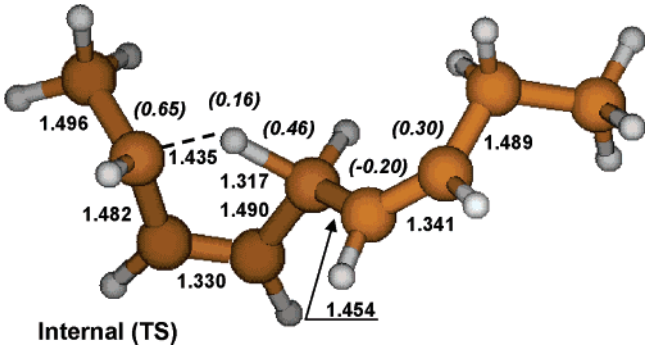

Figure 6. Optimized transition structure in the H transfer reaction between the allylic NDE(C_8) and pentadienylic NDE(C_{11}) radicals (Figure 2). Distances in Å. Spin distributions (au) given in parentheses.

mol for addition to C_{11}. Inclusion of free energy corrections and solvent effects hence leads to a considerable increase in barrier heights, whereas the gas-phase adiabatic data is fully in agreement with the data reported earlier for the propargyl and allyl radiacls.[38,39]

3.2.2. Addition to the mono-Allylic Methylene NDE(C_8). Also, for NDE(C_8), two addition sites are possible, to C_8 (pathway NDE(C_8) + O_2 → **12** → **13** → **14**) or to C_{10} (pathway NDE(C_8) + O_2 → **15** → **16** → **17**), differing in that C_{10} is bonded to a bridging methylene group (C_{11}) connecting the two conjugated fragments (see Figure 5). The two reactant complexes (**12** and **15**) have very similar local features, with two unpaired electrons on the molecular oxygen, a C···O distance of 3.4−3.6 Å, and essentially an unaltered structure and spin distribution of the carbon-centered radical compared with the isolated case (NDE(C_8)). Larger differences are seen between the two transition state structures **13** and **16**, in that TS **13** leading to C_8 addition is much later. This is reflected in the shorter C···O distance (1.9 vs 2.1 Å), the smaller delocalization of the unpaired spin on both the oxygen moiety and the carbon fragment, and the larger changes in C−C bond lengths (C_8−C_9 increasing by 0.07 Å in TS **13** with respect to **12**; while the largest change in TS **16** with respect to **15** is seen for C_9−C_{10}, increasing by 0.03 Å). For the two product complexes **14** and **17**, respectively, the situations closely resemble that of the previously discussed adduct **11**, with unpaired spin 0.71 and 0.28 electrons on the two oxygen atoms and localized double bonds in the lipid fragment.

Energetically (Table 2), TS **13** also stands out as being different from the rest. Whereas TS **16** has a MPWB1K/MG3S + ZPE potential energy barrier of 13.8 kcal/mol, that for TS **13** is only 1.7 kcal/mol at the same level. The Gibbs free energy barriers when including the CPCM solvent corrections are 9.9 and 14.5 kcal/mol for TS **13** and TS **16**, respectively. In all, it thus appears that O_2 addition to C_8 in the allylic lipid radical system is a faster reaction than any of the others. The two product complexes **14** and **17** have very similar energies, and are 5−10 kcal/mol more stable than the adducts for addition to the pentadienyl radical discussed above. The effects of the different functionals (B3LYP and BH&HLYP) on the barrier heights are very similar to those discussed for the H abstraction reactions.

3.3. Internal H Transfer. The two H abstraction radicals NDE(C_{11}) and NDE(C_8) studied in the current model differ in the length of the conjugated radical fragment (three or five carbons, respectively). The increased conjugation of the pentadienyl radical NDE(C_{11}) renders this to be more stable than the allylic one, by 5.4 kcal/mol (MPWB1K/MG3S + ZPE level). The Gibbs free energy difference between the two is 3.3 kcal/mol at the CPCM-MPWB1K/MG3S level. The species with extended conjugation is mainly attributed to the observed peroxyl products, albeit our computed energies of OH-radical-induced hydrogen abstraction indicate that formation of the allylic radical is associated with a slightly lower barrier and that O_2 addition will preferentially occur at the C_8 carbon of the allylic radical NDE(C_8). A possibility for this discrepancy could be internal transfer of a hydrogen atom from C_{11} to C_8 in the allylic species, thereby generating the pentadienyl radical NDE(C_{11}).

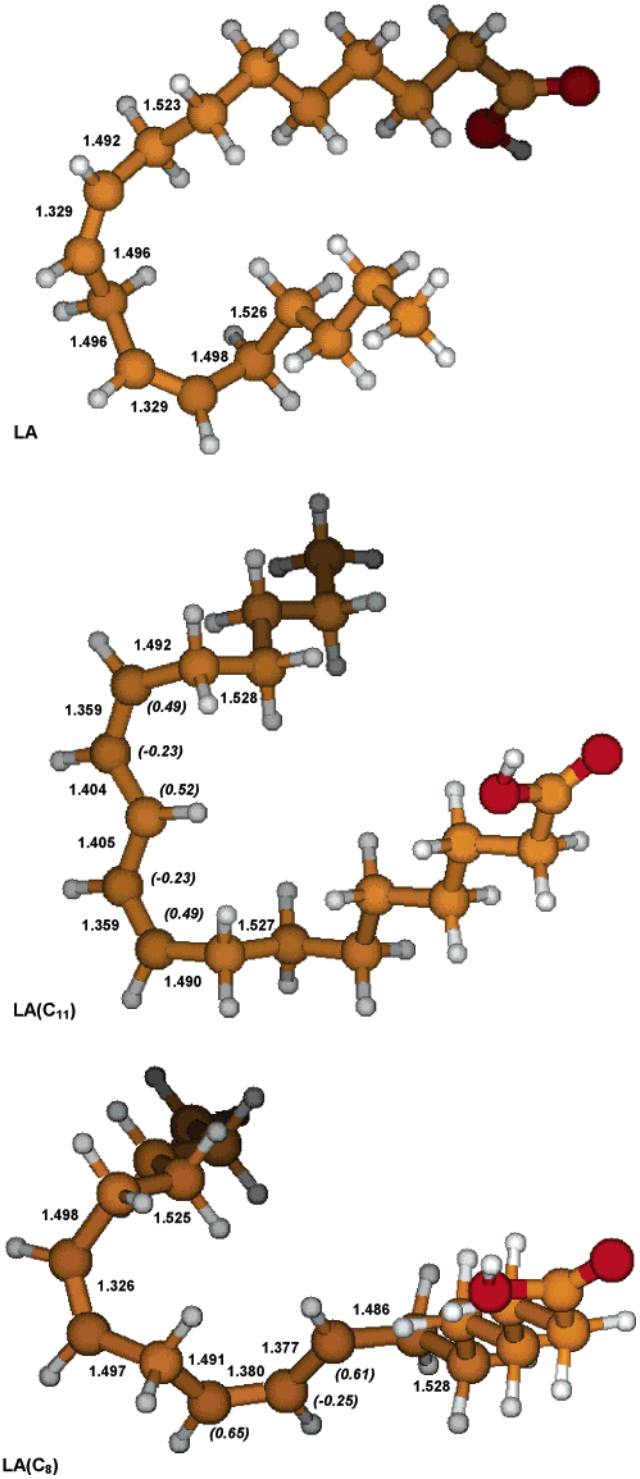

Figure 7. Optimized structures of linoleic acid (LA) and the pentadienylic LA(C_{11}) and allylic LA(C_8) H abstraction radicals. Distances in Å. Spin distributions on the carbon atoms (au) given in parentheses.

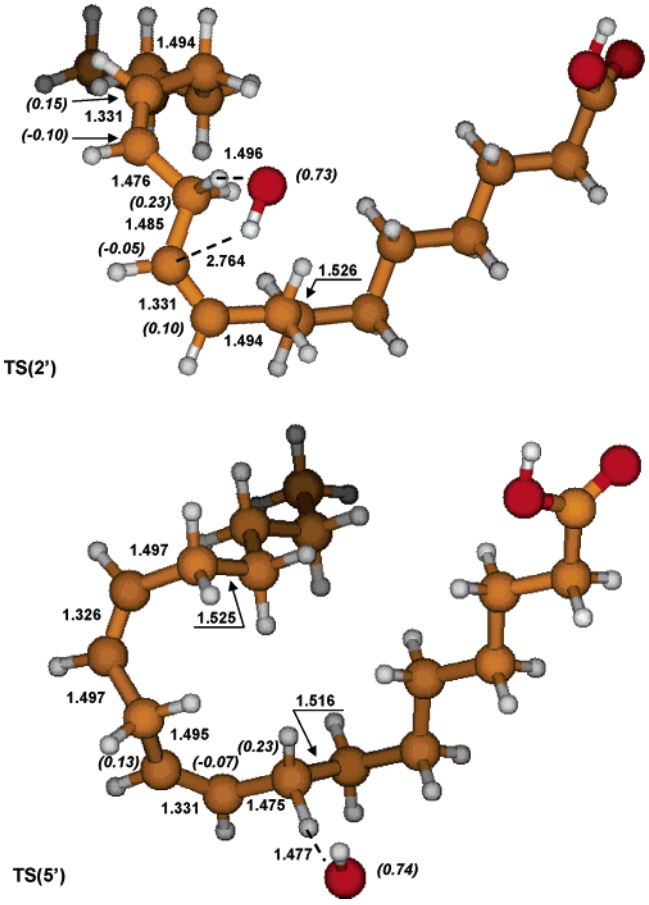

Figure 8. Optimized transition state structures for OH-induced H abstraction: TS **2′** from bis-allylic C_{11} in LA(C_{11}H) and TS **5′** from C_8/C_{14} in LA(C_8H). Distances in Å. Spin distributions (au) given in parentheses.

In Figure 6, we show the optimized transition state structure connecting the two H abstraction radicals NDE(C_8) and NDE(C_{11}). The hydrogen atom to be transferred is close to the midpoint between the carbons, albeit somewhat closer to C_{11} (R_{H-C11} = 1.317 Å; R_{H-C8} = 1.435 Å). The C−C distances also undergo large changes going from NDE(C_8) to the internal TS. R_{C8-C9} is changing from an allylic π-bond to a bridging σ-bond, and is already in the TS close to its corresponding value in the radical product NDE(C_{11}). The neighboring C_9-C_{10} bond changes temporarily toward a pure π-bond in the TS, with a shorter bond length (1.330 Å) than that in either the allyl or pentadienyl radical, and the C−C bonds in the $C_{11}-C_{14}$ fragment lie essentially halfway between those found in NDE(C_8) and NDE(C_{11}). The main fraction of the unpaired spin is in the TS shared between the reacting carbons C_8 and C_{11}, with slight components also on the transferring hydrogen atom and on C_{12} and C_{13}.

The transition state structure lies very high in energy, around 38 kcal/mol above the reactant NDE(C_8), both at the zero-point-corrected MPWB1K/MG3S level and at the CPCM-MPWB1K/MG3S Gibbs free energy level. We may hence conclude that internal H atom transfer to generate an extended conjugated species is not likely to occur. Instead, it appears that thermodynamics or possibly effects from the local surroundings govern the preference for formation of NDE(C_{11}) over NDE(C_8).

3.4. The Effect of a Larger Lipid Model in the OH-Radical-Induced H Abstraction. At this point, the computational results show that the H abstraction, as the initial event in the lipid peroxidation process, has a lower kinetic barrier when the OH radical attacks the mono-allylic methylene group (C_8/C_{14}) than when the hydrogen abstraction is at the bis-allylic site (C_{11}). Despite the latter being a more exergonic reaction, the 3.2 kcal/mol of difference in Gibbs free energy barriers reveals two very competitive mechanisms. Hence, there seems to be an interesting contrast between the data for the NDE model system and what is suggested as the general lipid peroxidation initiation mechanism.

The steric factors of the surroundings can be crucial in order to entropically disfavor hydrogen abstraction at the mono-allylic methylene position with respect to the one at the bis-allylic site. For this reason, we carried out calculations of the initiation step explicitly including the whole linoleic acid as our lipid model (21 heavy atoms). The reactant and product complexes were neglected due to the computational cost and also because they vanish when considering the Gibbs free energies.

The optimized structures, key geometric parameters, and spin distributions of the new lipid model and their corresponding H abstraction radicals are depicted in Figure 7. The same information is shown in Figure 8 for the transition state structures connecting LA with each LA radical.

All of the optimized C−C distances for LA, transition state structures, and LA radicals are very similar (variations being less than $^1/_{10}$ of an angstrom) to the ones obtained when employing the NDE model. The main geometric differences between the two models come from the distances participating in the transition vector and also from the orientation of the nonconjugated double bonds. The dihedral angle between the latter is approximately 90° in the free NDE model but around 45° in LA.

In going from reactants to a more delocalized structure through hydrogen abstraction at the bis-allylic site (pathway LA(C_{11}H) + OH → **1′** → **2′** → **3′** → LA(C_{11}) + H_2O), TS **2′** has its double bonds in more of a *cis* disposition (20°) than the corresponding free LA. In contrast, the TS **2** corresponding to the smaller lipid model has a more *trans* disposition (120°) than the free NDE. Both LA(C_{11}) and NDE(C_{11}) structures have a

TABLE 3: Energetics (in kcal/mol) for the H Abstractions Studied Using Linoleic Acid (LA) (Reactant and Product Complexes, in Brackets, Not Included)

reaction	compound	ΔE_{ZPE}[a] MPWB1K	$\Delta G^{298}_{lip.}$[b] MPWB1K
H abstraction on C_{11}:	LA(C_{11}H) + OH•	0.0	0.0
LA(C_{11}H) + OH → [1′] → 2′ → [3′] → LA(C_{11}) + H_2O	TS **2′**	−1.1	7.6
	LA(C_{11})• + H_2O	−44.6	−47.5
H abstraction on C_8/C_{14}:	LA(C_8H) + OH•	0.0	0.0
LA(C_8H) + OH → [4′] → 5′ → [6′] → LA(C_8) + H_2O	TS **5′**	−0.2	8.9
	LA(C_8)• + H_2O	−34.2	−39.4

[a] Gas-phase calculations. [b] CPCM (ϵ = 4) calculations.

planar disposition of the pentadienyl radical, but the original nonconjugated double bonds are in a *trans*−*trans* and *trans*−*cis* disposition for the most stable LA and NDE models, respectively. For the TS **2′**, the $R_{C-H} = 1.116$ Å and $R_{O-H} = 1.496$ Å values corresponding to the transition vector are both smaller (by 0.02 and 0.07 Å, respectively) than in the NDE model. Despite the use of a larger lipid model, the disposition of the nonconjugated double bonds gives rise to less steric hindrance in the reactant site and allows for a more compressed transition state structure.

For the other hydrogen abstraction pathway ($LA(C_8H) + OH \rightarrow$ **4′**$\rightarrow$ **5′** $\rightarrow$ **6′** $\rightarrow LA(C_8) + H_2O$), the geometrical differences when comparing the LA and NDE models follow a similar behavior as described above. In this case, the dihedral angle between nonconjugated bonds observed in the optimized LA structure preserves the same value in the TS **5′** as well as in the $LA(C_8)$ structures. This conserved geometrical parameter along the pathway was also observed for the NDE model. As a consequence, the new formed carbyne group in $LA(C_8)$ is *cis* with respect to the rest of the allyl group, whereas for the shorter lipid model the orientation was *trans*. For TS **5′**, the $R_{C-H} = 1.157$ Å value is a little bit longer (0.01 Å) and the $R_{O-H} = 1.477$ Å value is smaller (0.05 Å) than the values for the NDE TS **5**. These distances still maintain the sterical criteria discussed for the previous mechanism.

In Table 3, we show the gas-phase adiabatic energies including ZPE corrections and the Gibbs free energies in solution, both obtained at the MPWB1K/MG3S level and using the new lipid model. The Gibbs free energy barrier of hydrogen abstraction at the bis-allylic site is 7.6 kcal/mol (4.6 kcal/mol less than when using the NDE model), whereas the corresponding barrier for hydrogen abstraction at the mono-allylic site is now 8.9 kcal/mol (1 kcal/mol higher than for the shorter lipid model). Both mechanisms become more exergonic and favor even more the most accepted initiation mechanism than when the NDE model was employed. The different conclusions reached when using the full lipid as a model, or just the reactant part of it, emphasizes the great importance of the local surrounding in the working model. It appears that the main source of this difference arises from the more compact TS structures obtained with the larger model, along with the somewhat different conformational orientations generated within the two models.

4. Conclusions

In this paper, we have theoretically studied the OH-radical-induced peroxidation of linoleic acid by exploring the corresponding MPWB1K/MG3S//MPWB1K/6-31+G(d,p) potential energy surfaces. We have also estimated the solvation effects calculating Gibbs free energies by means of the CPCM method. We have first studied the possible OH-induced hydrogen abstractions from nona-3,6-diene (taken as a model of the linoleic acid) and the subsequent possible triplet O_2 additions leading to peroxyl radical formation.

Conversely to the experimental results, our calculations on NDE indicated that hydrogen abstraction at the mono-allylic methylene groups (C_8/C_{14}) is easier than at the bis-allylic site (C_{11}). However, when the whole linoleic acid is considered in the calculations, hydrogen abstraction from the C_{11} atom becomes the most favorable, in good agreement with experiment. Our results in this paper shed light on the mechanism of the OH-induced lipid peroxidation reaction and highlight the need to choose a sufficiently complete model of the real system in order to obtain reliable theoretical results.

Acknowledgment. We are grateful for financial support from the Spanish "Ministerio de Educación y Ciencia", the "Fondo Europeo de Desarrollo Regional" through project CTQ2005-07115/BQU, the "DURSI de la Generalitat de Catalunya" (2005SGR00400), the Swedish Science Research Council (VR), and the Faculty of Medicine, Science and Technology (MNT) at Örebro University.

References and Notes

(1) Halliwell, B.; Gutteridge, J. M. C. *Free Radicals in Biology and Medicine*, 3rd ed.; Oxford University Press: Oxford, U.K., 1999.
(2) Niki, E.; Yoshida, Y.; Saito, Y.; Noguchi, N. *Biochem. Biophys. Res. Commun.* **2005**, *338*, 668.
(3) Wiseman, H.; Halliwell, B. *Biochem. J.* **1996**, *313*, 17.
(4) Vaca, C. E.; Wilhelm, J.; Harmsringdahl, M. *Mutat. Res.* **1988**, *195*, 137.
(5) Steinberg, D.; Parthasarathy, S.; Carew, T. E.; Khoo, J. C.; Witztum, J. L. *N. Engl. J. Med.* **1989**, *320*, 915.
(6) Esterbauer, H.; Gebicki, J.; Puhl, H.; Jurgens, G. *Free Radical Biol. Med.* **1992**, *13*, 341.
(7) Spiteller, P.; Spiteller, G. *Chem. Phys. Lipids* **1997**, *89*, 131.
(8) Noguchi, N.; Yamashita, H.; Hamahara, J.; Nakamura, A.; Kuhn, H.; Niki, E. *Biol. Chem.* **2002**, *383*, 619.
(9) Sloane, D. L.; Leung, R.; Craik, C. S.; Sigal, E. *Nature* **1991**, *354*, 149.
(10) Tejero, I.; Eriksson, L. A.; Gonzalez-Lafont, A.; Marquet, J.; Lluch, J. M. *J. Phys. Chem. B* **2004**, *108*, 13831.
(11) Wrona, M.; Korytowski, W.; Roznowska, M.; Sarna, T.; Truscott, T. G. *Free Radical Biol. Med.* **2003**, *35*, 1319.
(12) Stratton, S. P.; Liebler, D. C. *Biochemistry* **1997**, *36*, 12911.
(13) Tejero, I.; Gonzalez-Lafont, A.; Lluch, J. M.; Eriksson, L. A. *Chem. Phys. Lett.* **2004**, *398*, 336.
(14) Cosgrove, J. P.; Church, D. F.; Pryor, W. A. *Lipids* **1987**, *22*, 299.
(15) Gardner, H. W. *Free Radical Biol. Med.* **1989**, *7*, 65.
(16) Esterbauer, H.; Schaur, R. J.; Zollner, H. *Free Radical Biol. Med.* **1991**, *11*, 81.
(17) Fink, S. P.; Reddy, G. R.; Marnett, L. J. *Proc. Natl. Acad. Sci. U.S.A.* **1997**, *94*, 8652.
(18) Salomon, R. G.; Kaur, K.; Batyreva, E. *Trends Cardiovasc. Med.* **2000**, *10*, 53.
(19) Yin, H. Y.; Havrilla, C. M.; Morrow, J. D.; Porter, N. A. *J. Am. Chem. Soc.* **2002**, *124*, 7745.
(20) Spiteller, G. *Chem. Phys. Lipids* **1998**, *95*, 105.
(21) Pignatello, J. J.; Oliveros, E.; MacKay, A. *Crit. Rev. Environ. Sci. Technol.* **2006**, *36*, 1.
(22) Uchino, T.; Tokunaga, H.; Ando, M.; Utsumi, H. *Toxicol. in Vitro* **2002**, *16*, 629.
(23) Ali, H.; van Lier, J. E. *Chem. Rev.* **1999**, *99*, 2379.
(24) Hideg, E.; Vass, I. *Plant Sci.* **1996**, *115*, 251.
(25) von Sonntag, C. *The Chemical Basis of Radiation Biology*; Taylor & Francis: London, 1987.
(26) Matxain, J. M.; Ristilä, M.; Strid, Å.; Eriksson, L. A. *J. Phys. Chem. A* **2006**, *110*, 13068.
(27) Shustov, G. V.; Spinney, R.; Rauk, A. *J. Am. Chem. Soc.* **2000**, *122*, 1191.
(28) Kohn, W.; Becke, A. D.; Parr, R. G. *J. Phys. Chem.* **1996**, *100*, 12974.
(29) Becke, A. D. *J. Chem. Phys.* **1993**, *98*, 5648.
(30) Wang, Y.; Perdew, J. P.; Chevary, J. A.; Macdonald, L. D.; Vosko, S. H. *Phys. Rev. A* **1990**, *41*, 78.
(31) Becke, A. D. *J. Chem. Phys.* **1996**, *104*, 1040.
(32) Zhao, Y.; Truhlar, D. G. *J. Phys. Chem. A* **2004**, *108*, 6908.
(33) Zhao, Y.; Truhlar, D. G. *J. Phys. Chem. A* **2005**, *109*, 5656.
(34) Taghikhani, M.; Parsafar, G. A.; Sabzyan, H. *J. Phys. Chem. A* **2005**, *109*, 8158.
(35) Lynch, B. J.; Zhao, Y.; Truhlar, D. G. *J. Phys. Chem. A* **2003**, *107*, 1384.
(36) Barone, V.; Cossi, M. *J. Phys. Chem. A* **1998**, *102*, 1995.
(37) Frisch, M. J.; Trucks, G. W.; Schlegel, H. B.; Scuseria, G. E.; Robb, M. A.; Cheeseman, J. R.; Montgomery, J. A., Jr.; Vreven, T.; Kudin, K. N.; Burant, J. C.; Millam, J. M.; Iyengar, S. S.; Tomasi, J.; Barone, V.; Mennucci, B.; Cossi, M.; Scalmani, G.; Rega, N.; Petersson, G. A.; Nakatsuji, H.; Hada, M.; Ehara, M.; Toyota, K.; Fukuda, R.; Hasegawa, J.; Ishida, M.; Nakajima, T.; Honda, Y.; Kitao, O.; Nakai, H.; Klene, M.; Li, X.; Knox, J. E.; Hratchian, H. P.; Cross, J. B.; Adamo, C.; Jaramillo, J.; Gomperts, R.; Stratmann, R. E.; Yazyev, O.; Austin, A. J.; Cammi, R.; Pomelli, C.; Ochterski, J. W.; Ayala, P. Y.; Morokuma, K.; Voth, G. A.;

Salvador, P.; Dannenberg, J. J.; Zakrzewski, V. G.; Dapprich, S.; Daniels, A. D.; Strain, M. C.; Farkas, O.; Malick, D. K.; Rabuck, A. D.; Raghavachari, K.; Foresman, J. B.; Ortiz, J. V.; Cui, Q.; Baboul, A. G.; Clifford, S.; Cioslowski, J.; Stefanov, B. B.; Liu, G.; Liashenko, A.; Piskorz, P.; Komaromi, I.; Martin, R. L.; Fox, D. J.; Keith, T.; Al-Laham, M. A.; Peng, C. Y.; Nanayakkara, A.; Challacombe, M.; Gill, P. M. W.; Johnson, B.; Chen, W.; Wong, M. W.; Gonzalez, C.; Pople, J. A. *Gaussian 03*, revision B.04; Gaussian, Inc.: Pittsburgh, PA, 2003.

(38) Dong, F.; Wang, S. F.; Kong, F. A. *J. Phys. Chem. A* **2003**, *107*, 9374.

(39) Hahn, D. K.; Klippenstein, S. J.; Miller, J. A. *Faraday Discuss.* **2001**, *119*, 79.